International Journal of Materials and Chemistry 2013, 3(5): 106-111
DOI: 10.5923/j.ijmc.20130305.04

Synthesis, Characterization and Magnetic Properties of γ-irradiated and Unirradiated Magnetite Nanopowders

M. Khairy

Chemistry Department, Faculty of Science, Benha University, Benha, Egypt

Abstract Nano-sized magnetite (Fe_3O_4) nanoparticles were prepared using dry and wet chemical methods in presence of surfactants as capping agents. The samples were characterized by X-ray diffraction, FT-IR, thermal analysis (DTA and TG), Electron microscopy (SEM) as well as (TEM), dynamic laser scattering analyzer (DLS) and vibrating sample magnetometer (VSM) techniques. The X-ray diffraction pattern show cubic spinel crystal structure for all samples. Particle size in the range of 8 - 55 nm is obtained. The effect of preparation method and γ- irradiation process on the magnetic properties of prepared samples was studied and discussed. All samples show soft-magnetic behavior with much lower coercivity and much higher saturation magnetization. The coercive force (H_c), saturation magnetization (B_s), remanent induction (B_r) and the ratio of remanent induction to saturation magnetization (B_r/B_s) are found to be size and shape dependent. The saturation magnetization value lies between 20.5 and 64.5 emu/g. The magnetic properties are explained by electron hopping mechanism between Fe^{2+} and Fe^{3+} -ions. The use of magnetite nanoparticles in preparation of ferrofluid was investigated. The ferrofluid stability increases with decreasing the particle size.

Keywords Nanostructures, Magnetite, VSM, Gamma Irradiation, Magnetic Properties

1. Introduction

Over the past few years, controlling the size and shape of metal oxides has attracted significant interest because the shape and size of these materials have significant influence on their chemical and physical properties[1-4]. Magnetite (Fe_3O_4), as one kind of important transition metal oxides, is of particular importance because of both its unique properties including magnetic properties, chemical stability, biocompatibility, and low toxicity and potential applications in magnetic recording and separation, catalyst, photocatalyst, pigments, ferrofluids, magnetic resonance imaging (MRI), drug delivery, etc.[5-8].

There are several methods have been developed to synthesize Fe_3O_4 nanoparticles[9]. However, the shape controlled synthesis of Fe_3O_4 in the nanometer regime has limited success. The size and morphology of nanoparticles are two important characteristic influencing their electrical, optical and magnetic properties[10-13]. The difference between nano and bulk materials has immense theoretical and technological importance. The way nanoparticles are synthesized may determine their morphological uniformity and size distribution; these conditions become one of the key challenging issues in nanoscience and nanotechnology[13]. Most commonly, Fe_3O_4 nanoparticles are prepared via co-precipitating ferrous and ferric ions in aqueous solution[14]. However, the corresponding chemical reactions do occur very fast, just promptly on mixing reactants, and this makes it very difficult to control the crystallization process. As a consequence, the magnetic nanoparticles of the resulting iron oxides tend to exhibit relatively poor size uniformity and crystallinity, and this feature may limit their use in many technological applications.

Ionizing radiation such as gamma ray has frequently been used in studies of the physical properties of crystalline solids[15]. Structural defects can be introduced by ionizing radiation. Severe disruption of the lattice of a crystalline solid is possible, with the formation of a large number of defects. In this context, in the present investigation, dry and wet chemical methods have been employed to synthesized Fe_3O_4 powders with an average particle size down to several nanometers. The XRD, FTIR, SEM and TEM techniques were used to characterize the structure, purity, and the size of the nanoparticles. The magnetic properties were evaluated by vibrating sample magnetometer (VSM) measurement. The magnetization curves of these nanocrystals have been tested and analyzed. The relationship between preparation methods and the magnetic properties of resulting materials identified via the above methods was discussed. The influence of gamma ray on the magnetic properties of the synthesized nanoparticles was examined. The investigated Fe_3O_4 nanoparticles were dispersed into aqueous citric acid

* Corresponding author:
moh_khairy3@yahoo.com (M. Khairy)
Published online at http://journal.sapub.org/ijmc

to obtain nanofluids and their stabilities were tested.

2. Experimental

2.1. Materials

Analytical pure ferrous nitrate ($Fe(NO_3)_2 \cdot 4H_2O$), Ferric nitrate ($Fe(NO_3)_3 \cdot 9H_2O$), ferrous oxalate dihydrate ($FeC_2O_4.2H_2O$), ammonium hydroxide (NH_4OH, 28–30% of ammonia), 1-adamantanecarboxylic acid (ACA, 99%), and cetylpyridinium bromide (CPB) were purchased from Aldrich and used for Fe_3O_4 synthesis.

2.2. Synthesis of Magnetite Nanoparticles

The magnetite samples were prepared using both thermal decomposition and wet chemical methods in the presence and absence of surfactants as follows:

(a) Wet chemical method

Fe_3O_4 nanoparticles were synthesized according to the coprecipitation method. A typical preparation process is described as following: a definite weights of $Fe(NO_3)_2 \cdot 4H_2O$ (21.4 g) and $Fe(NO_3)_3 \cdot 9H_2O$ (28.9 g) were dissolved in distilled water in presence of 10 mmol surfactant (50 ml) with a nitrogen protection. After the solution had been bubbled with nitrogen for 30 min, 0.1 mol/L NH_4OH solution was introduced slowly into the system to adjust the pH above 11. The system was continuously bubbled with nitrogen for 20 min to remove oxygen. The formed black precipitates were collected from the solution by centrifugation, washed with distilled water several times, and dried at 90℃ for 8 h. The composition of Fe_3O_4 was verified by $KMnO_4$ titration method[16]. The results showed a ratio of Fe^{3+}: Fe^{2+} agrees with the expected 2:1 ratio within 2%.The samples were denoted as S for the sample prepared without surfactant and as S_{CPB} and S_{ACA} for the samples prepared using CPB and ACA surfactants, respectively.

(b) Thermal decomposition dry method

For the dry method, 10 g of ferrous oxalate dihydrate was thermally decomposed, at low oxygen partial pressure, for 6 h at T=773 K[17]. The obtained product was then milled in a planetary ball mill. The milling was performed in a closed container with a hardened-steel vial of 120 ml volume and 80 hardened-steel with a diameter of 10 mm at ambient temperature. The milling intensity was 200 rpm and the ball-to-powder weight ratio of 20:1 was chosen. The milling process was carried out for one hour. The sample is denoted as S_d.

All dry magnetite samples were kept in desiccators over calcium chloride to avoid the oxidation to maghemite. The prepared samples were irradiated by γ-ray source using a ^{60}Co gamma cell (^{60}Co gamma cell 2000 Ci with a dose rate of 1.5 Gy/s (150 rad/s) at a temperature of 30℃. Each sample was subjected to a total final dose of $1x10^5$ Gy (10 Mrad). The irradiated samples were distinguished from the unirradiated ones by adding an asterisk beside the symbol of the irradiated samples, e.g. S_d*.

For preparing aqueous based ferrofluids, one gram from each one of γ-irradiated and unirradiated magnetite samples was suspended in 10 ml of 50 wt% aqueous citric acid and heated at 90°C for 90 minutes under vigorously mechanically stirring.

2.3. Instrumentation and Measurements

Thermal analysis (DTA and TG), XRD, FT-IR, SEM and TEM techniques were employed to characterize thermal stability, structure and morphology of the investigated magnetite samples. The thermal analysis was recorded using Schimadzu DT-50 thermal analyzer with samples of about mg in a static air atmosphere and at heating rate 10 K/min. The thermograms showed thermal stability for all samples over a temperature range of 300 - 673 K. Phase identification of the prepared samples was carried out at room temperature by X-ray diffraction (XRD) patterns using a Philips diffractometer PW 1710 with Cu-Kα irradiation (λ=0.15405 nm). FT-IR spectra were performed by FT-IR spectrophotometer model Perkin-Elmer 599 using KBr pellet technique. Scanning electron microscopy (SEM) and Transmittion electron microscopy (TEM) were taken using electron microscope models JEM-5200 Joel and Joel 2010 respectively. The volume-average diameter and size distribution of Fe_3O_4 magnetic nanoparticles in ethanol were measured by dynamic light scattering (DLS) using Malvern HPPS5001 laser particle-size analyzer at 25℃. Magnetic measurements were measured at room temperature using a vibrating sample magnetometer (VSM; 9600-1 LDJ, USA) in a maximum applied field of 15 kOe. Sedimentation method was used to test the ferrofluid stability of the studied samples. The sedimentation under gravity was carried out as described by Thies-Weesie et al.[18]. Weighted amounts of the ferrofluids were poured into cylindrical glass tubes of 1 cm diameter and 15 cm length and carefully closed. The tubes were vertically immersed in a water bath, placed on a heavy marble table to minimize vibrations. The equipment was placed in a thermostatic room to keep the temperature of the sedimentation dispersions constant at 25.0(0.1℃).

3. Results and Discussion

3.1. Characterization of the samples

X-ray diffraction patterns of the synthesized Fe_3O_4 samples are shown in Fig. 1. All the observed peaks agree well with the corresponding reported JCPDS file (19-629) for the magnetite spinel structure. The crystallites sizes, D_{XRD}, were estimated by using the Scherrer's equation[19], based on (311) peak: $D_{XRD} = 0.9\,\lambda / \beta \cos\theta$ where λ is the X-ray wave length, θ the Bragg's angle and β is the pure full width of the diffraction line at half of the maximum intensity. D_{XRD} values obtained lie in the range of 8 - 55 nm, Table 1. The irradiated samples also exhibit the same crystalline phase with crystallite sizes in the same order with that found

for unirradiated ones.

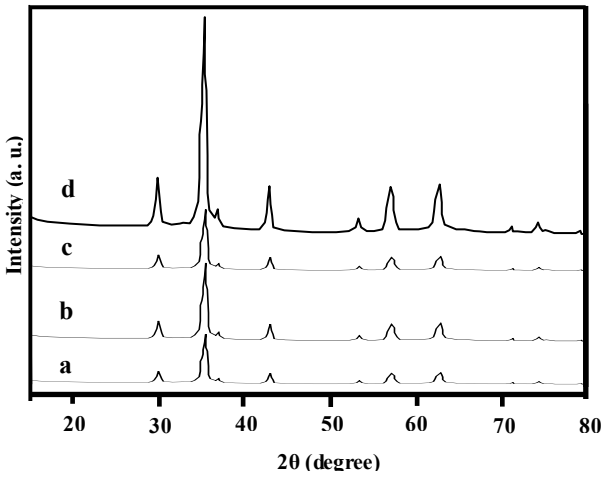

Figure 1. XRD patterns of Fe_3O_4 samples: a)S b) S_d c) S_{CPB} d) S_{ACA}

Table 1. Particle size and FT-IR data of γ-irradiated and unirradiated nano magnetite samples

samples	Particle size (TEM), nm	Particle size (XRD), nm	υ_o cm^{-1}	υ_t cm^{-1}
S	52	55	384	560
S*	47	51	388	564
S_{CPB}	27 (diameter)	38	391	568
S_{CPB}*	23 (diameter)	33	395	571
S_d	19	16	399	571
S_d*	17	13	401	575
S_{ACA}	9(diameter)	10	405	578
S_{ACA}*	8(diameter)	8	408	583

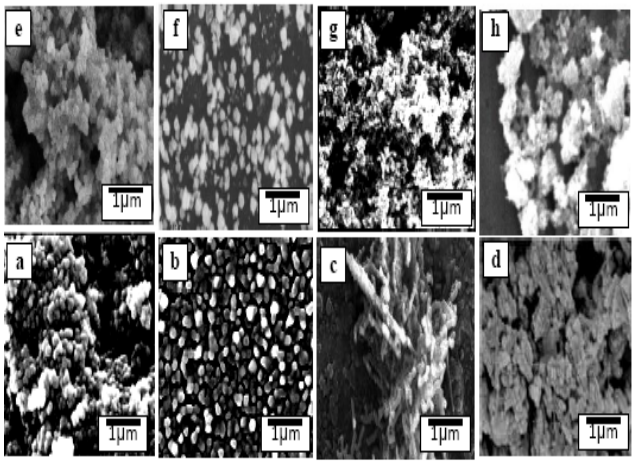

Figure 2. SEM micrographs of: a)S b) S_d c) S_{CPB} d) S_{ACA} e)S* f) S_d* g) S_{CPB}* h) S_{ACA}*

Figs. 2a-e shows the scanning electron micrographs (SEM) of γ- irradiated and unirrdiated samples. The morphology of the particles is found to depend on both the type of surfactant and the preparation method used. The SEM images of S and S_d show surface morphology consisting of nearly spherical like structure. On the other side, the images of S_{ACA} and S_{CPB} reveal spread of somehow aggregates of granular particles with random shapes. This reflects the role of surfactants as capping agent in controlling the growth rate of various faces of Fe_3O_4 crystal. The SEM of irradiated samples show surface morphologies almost similar to that observed for unirradiated ones. This reflects the insignificant influence of the formed lattice defects, during the irradiation process, on the morphologies of the magnetite specimens.

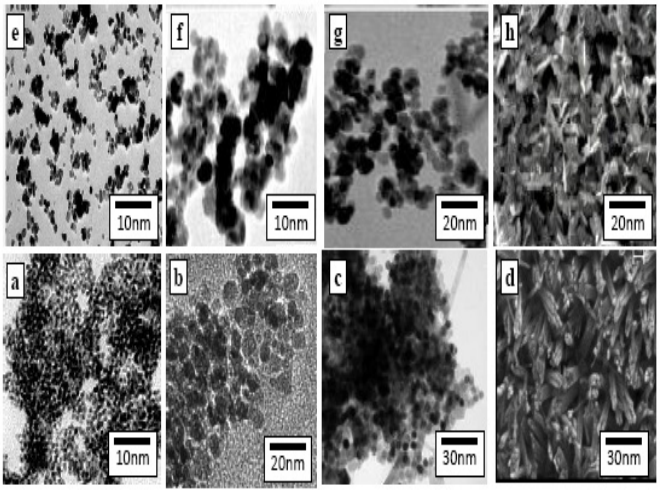

Figure 3. TEM micrographs of: a)S b) S_d c) S_{CPB} d) S_{ACA} e)S* f) S_d* g) S_{CPB}* h) S_{ACA}*

The morphologies of Fe_3O_4 particles were further investigated by TEM, Fig. 3. The TEM images confirm clearly the formation of nano scale magnetite particles. Both of the shape and particle size were also found to depend on the preparation method. The TEM images of S and S_d samples show that the Fe_3O_4 particles consist of agglomerated shapes of deformed spheres with an average diameter of 52 and 19 nm, respectively. Usually, spherical shapes are formed when the nucleation rate per unit area is isotopic at the interface between the Fe_3O_4 magnetic nanoparticles. Minimization of the surface free energy by reduction of total surface area/volume, results in the equivalent growth rate along different directions of the nucleation because the sphere has the smallest surface area per unit volume of any shape. The TEM images for the samples prepared in presence of surfactants S_{ACA} and S_{CPB} (Figs. 3(c,d,g,h)) show particles with nano rods structure with diameter of 9 nm and length of 0.69 μm as well as 27 nm and length of 3 μm, respectively. These nano rods are a good evidence of ″oriented attachment 'growth, in which the individual particles were aligned like a wall, whereas the second layer of bricks were about to be put on the first. The difference between the crystallite sizes estimated by the Sherrer's formula and that found by TEM images (Table 1) is mainly attributed to the different approach of two techniques. In XRD, we determine the mean particle size using a shape factor of 0.9. This factor is depended on the shape of the particle used and is not definite determined. Therefore, any change in the shape factor will cause a change in the particle size calculated.

The analysis of the particles using dynamic light scattering (DLS) showed that the magnetite particles are well dispersed

in ethanol, and the mean particle sizes obtained agree with those found by XRD and the TEM results for the spherical particles of S and Sd samples. On the other hand, the DSL analysis of SACA and SCPB with nano rod morphology showed particle sizes of ~12 and ~ 42 nm, respectively, which agree well with that found by XRD and differ than that found by TEM. This is attributed to that the DSL results show the hydrodynamic dimension from measuring the diffusion coefficient of the particle[20]. This coefficient is not only dependent on the mass of the particle, but also the shape and the surface chemistry of the particles because these parameters affect the particle-solvent interactions, and therefore, the Brownian motion of the particles.

For all the investigated samples, the FTIR spectra showed two main vibration bands for the iron-oxygen on both octal and tetrahedral positions (ν_O) and (ν_t) at 384-408 cm-1 and at 560-583 cm^{-1}[21], respectively. The peak positions of these modes vary with the particle size, Table 1. A principal effect of both finite sizes of nanoparticles is producing from the breaking of a large number of bonds for surface atoms, resulting in the rearrangement of localized electrons on the particle surface. As a result, the surface bond force constant increases as Fe_3O_4 is reduced to nanoscale dimensions, so that the absorption bands of IR spectra shift to higher wave numbers, as shown in our samples. The IR spectra of irradiated samples showed slight shift in band positions than that found for unirradiated ones. This may be attributed to the lattice defects producing in the magnetite after irradiation process.

3.2. Magnetic Properties

The basic property of any magnetic material is the relation between flux density and field strength. i.e. the B-H loop. For our samples, hysteresis loops with a normal (S-shape) type are observed at room temperature, Fig. 4 (a, b). The size and shape of the hysteresis curve are of considerable practical importance. The area within a loop represents a magnetic energy loss[22, 23]. This energy loss is defined as heat that is gratitude within the magnetic specimen and is capable of rising the temperature. The areas obtained for all samples are found to be small, and the loops are thin and narrow which is a specific criteria for soft ferrite. There is almost immeasurable coercivity at room temperature indicating that the prepared Fe_3O_4 samples are super paramagnetic. This super paramagnetic behavior means that the thermal energy can overcome the anisotropy energy barrier of a single Fe_3O_4 nano particle, and the coercivity and remanence of Fe_3O_4 nano particles are zero in the absence of external field. Saturation magnetic flux density (B_s), remnant magnetic flux density (B_r) and the ratio of remanent induction to saturation magnetization (B_r/B_s) were determined from B-H loops and listed in Table 2. From which it can be seen that the magnetic properties are size dependent. The coercivity H_c increases with increasing the crystallite size.

The saturation magnetization B_s ranges from 25.9 - 64.5 emu/g which are in all cases far from the reported values for bulk Fe_3O_4 (B_s= 92 emu/g)[22]. This decrease obtained in saturation magnetization value B_s can be understood on the basis of the increase occurring in the magnetically dead layer thickness (nonmagnetic or weakly magnetic interfaces) with the decreasing the crystallite size. With decreasing the particle size, the surface to volume ratio increases and in turn the magnetically dead layer fraction increases. Moreover, the magnetic spins of the surface molecules of nano particles are disordered due to the incomplete coordination, which may also be a reason for lower saturation magnetization. Generally, it can be said that the total magnetization of the sample decreases with decreasing particle size due to the increase in the magnetic integral[23-25] and ultimately reaches the super paramagnetic state, when each particle acts as a big spin with suppressed exchange interaction between particles. These might be the reasons for the magnetic moment quenching and consequently for the decrease in the saturation magnetization.

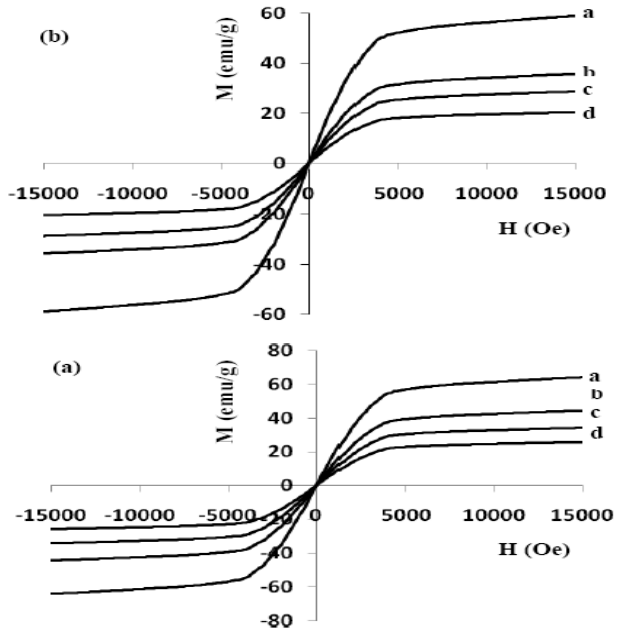

Figure 4a. Hysteresis curves at room temperature for unirradiated samples, a)S b) S_{CPB} c) S_d d) S_{ACA} **b.** Hysteresis curves at room temperature for irradiated samples, a)S* b) S_{CPB} * c) S_d * d) S_{ACA} *

The magnetization of γ-irradiated samples shows the same behavior as that found for unirradiated ones with a significant change in the magnetic parameters, Table 2. It is obvious that the magnetic values for irradiated specimens are less than that of unirradiated ones. These changes may be attributed to a change occurring in the Fe^{2+}/Fe^{3+} ratio after irradiation process, according to the following interaction [26]:

$$\gamma + Fe^{2+} \leftrightarrow Fe^{3+} + e$$

The obtained results may be also understood on the basis of crystal structure of Fe_3O_4. Magnetite (Fe_3O_4) is a ferrimagnetic iron oxide having cubic inverse spinel structure with oxygen anions forming an FCC closed packing and iron (cations) located at the interstitial

tetrahedral sites and octahedral sites[22]. The electron can hop between Fe^{2+} and Fe^{3+} ions in the octahedral sites at room temperature imparting half metallic property to magnetite. The magnetic moment of the unit cell comes only from Fe^{2+} ions with a magnetic moment of 4μB[27]. Therefore, the decrease in Fe^{2+}/Fe^{3+} ratio after irradiation process causes the decrease observed in Bs values for irradiated samples.

Table 2. Magnetic properties of the nano magnetite samples

Sample	D_{XRD} (nm)	H_c (Oe)	B_r (emu/g)	B_s (emu/g)	B_r/B_s ×100
S	55	114	1.03	64.5	2.02
S*	51	105	1.11	56.1	1.96
S_{CPB}	38	102	0.73	43.4	2.12
S_{CPB}*	33	78	0.59	35.1	1.68
S_d	16	77	0.33	34.0	0.97
S_d*	13	69	0.28	28.2	0.95
S_{ACA}	10	50	0.27	25.9	1.04
S_{ACA}*	8	36	0.21	20.5	1.02

3.3. Aqueous Ferro Fluid

A ferrofluid is a colloidal suspension of suitably coated magnetite particles in a liquid medium having unusual properties due to the simultaneous fluid mechanic effects and magnetic effects. Its wide spread applications are in the form of seals to protect high speed CD drives, as rotary shaft seals, for improving performance of audio speakers, in oscillation damping and position sensing[28], etc. A stable aqueous ferrofluid for our samples was prepared by dissolving the prepared nano particles in citric acid (used as dispersant) to form a stable aqueous dispersed magnetite particles, and simultaneously provide functional groups on the particle surface that can be used for further surface derivatization.

The behavior of ferrofluids is mainly determined by their magnetic properties. Usually, they show superparamagnetic behavior considering each particle as a thermally agitated permanent magnet in the carrier liquid. In the presence of a magnetic field, H, the magnetic moment (μ) of the particles will try to align with the magnetic field direction leading to a macroscopic magnetization of the liquid. The magnetization, M, of the liquid behaves as the magnetization of a paramagnetic system.

The stability of the ferrofluids prepared under the same conditions is found to depend on each of the particle size and morphology, Table 3. The samples with spherical particles (S and S_d) show higher stability than that of the other samples. Moreover, for the same morphology, the stability is found to increase with decreasing the particle size. The γ-irradiated samples show less stability than that of unirradiated ones. This is attributed to the smaller magnetic values of the irradiated specimens as compared with that of unirradiated ones.

4. Conclusions

The results show that Fe_3O_4 nanoparticles can be produced in the sizes range from 8 to 55 nm by dry and wet chemical methods. The sizes and the morphologies of magnetite particles are affected by the operational parameters. The magnetic properties of nanosized ferrites show an apparent superparamagnetic behavior and the magnetization is affected by γ- irradiation process. The magnetite particles have saturation magnetization values (B_s) ranging between 20.5 and 64.5 emu/g, which are far from the reported values for bulk Fe_3O_4 (B_s = 92 emu/g). The magnetic parameters (B_s, B_r and H_c) decrease with decreasing the particle size due to the existence of spin canting. Stable suspensions of magnetite nanoparticles in water (water-based ferrofluids) are prepared using citric acid as a dispersant. The stability of ferrofluids increases with decreasing the particle size of magnetite.

Table 3. Sedimentation data of ferrofluids sample

	Fe_3O_4	S_d	S_d*	S	S*	S_{ACA}	S_{ACA}*	S_{CPB}	S_{CPB}*
Time (h)					Height (cm)				
0		9.8	9.8	9.8	9.8	9.8	9.8	9.8	9.8
2		9.7	9.6	8.4	8.2	6.5	6.3	5	4.8
12		9.2	9	4.1	3.9	3.1	2.7	3	2.8
26		8.3	7.9	2.2	2.1	1.5	1.2	1	0.8
40		1	0.6	0.2	0.1	0.1	0.1	0	0
50		0	0	0	0	0	0		

REFERENCES

[1] R. Hallaj, K. Akhtari, A. Salimi, S. Soltanian, Controlling of morphology and electrocatalytic properties of cobalt oxide nanostructures prepared by potentiodynamic deposition method, Appl. Surf. Sci., 276 (2013) 512-520.

[2] C. Z. Yuan, H. B. Wu, Y. Xie, X. W. Lou, Intriguing mixed transition metal oxides: Design, controllable synthesis and energy-related applications, Angewan. Chem. Internat. Edition,DOI:10.1002/anie.201303971 (2013).

[3] N. V. Hieu, H. V. Vuong, N. V. Duy, N. D. Hoa, A morphological control of tungsten oxide nanowires by thermal evaporation method for sub-ppm NO_2 gas sensor application, Sens. Actuators B: Chem., 171–172, (2012)760-764.

[4] Z. Qin, T. Staudt, M. Happel, Y. Lykhach, M. Laurin, Sh. Shaikhutdinov, J. Libuda, A. Desikusumastuti, Controlling metal/oxide interactions in bifunctional nanostructured model catalysts: Pd and BaO on Al_2O_3/NiAl(110), Surf. Sci., 603 (2009) L9-L13.

[5] F. Jiao, J. C. Jumas, M. Womes, A. V. Chadwick, A. Harrison, P.G Bruce, Synthesis of ordered mesoporous Fe_3O_4 and γ-Fe_2O_3 with crystalline walls using post-template reduction/oxidation, J. Am. Chem. Soc., 128 (2006) 12905-12909.

[6] L.Y. Chen, Z.X. Xu, H. Dai, S.T. Zhang, Facile synthesis and magnetic properties of monodisperse Fe3O4/silica nanocomposite microspheres with embedded structures via a direct solution-based, J. Alloys Compd., 497 (2010) 221-227.

[7] S. H. Liu, R.M. Xing, F. Lu, R.K. Rana, J.J. Zhu, One-pot template-free fabrication of hollow magnetite nanospheres and their application as potential drug carrie, J. Phys. Chem. C, 113(2009) 21042-21047.

[8] Z. Lin, C. Zhao, Y. Zheng, Y. Zhou, H. Peng, Direct synthesis and characterization of mesoporous Fe_3O_4 through pyrolysis of ferric nitrate-ethylene glycol gel, J. Alloys Compd., 509 (2011) L1-L6.

[9] P. Enzel, N. Adelman, K.L. Beckman, Preparation and properties of an aqueous ferrofluid, J. Chem. Educ.,76 (1999) 943- 948.

[10] Y.Y. Zheng, X.B. Wang, L. Shang, C.R. Li, C. Cui, W.J. Dong, W.H. Tang, B.Y. Chen, Fabrication of shape controlled Fe_3O_4 nanostructure, Mater. Characteriz., 61 (2010) 489-492.

[11] Y.F. Shen, J. Tang, Z.H. Nie, Y.D. Wang, Y. Ren, L. Zuo, Tailoring size and structural distortion of Fe_3O_4 nanoparticles for the purification of contaminated water, Bioresource Technol.,100 (2009) 4139-4146.

[12] W. Bai, X. Meng, X. Zhu, Ch. Jing, Ch. Gao, J. Chu, Shape-tuned synthesis of dispersed magnetite submicro particles with good magnetic properties, Physica E, 42 (2009) 141-145.

[13] A. L. Andrade, M. A. Valente, J. M. F. Ferreira, J. D. Fabris, Preparation of size-controlled nanoparticles of magnetite, J. Magn. Magn. Mater., 324(10) (2012) 1753-1757.

[14] H. Meng, Z. Zhang, F. Zhao, T. Qiu, J. Yang, Orthogonal optimization designe for preparation of Fe_3O_4 nanoparticles via chemical coprecipitation, Appl. Surf. Sci., 280 (2013) 679.

[15] T. Tuner, M. Korkmaz, ESR study of ascorbic acid irradiated with gamma-rays, J. Radioanal. Nucl. Chem., 273 (2007) 609-614.

[16] A. I. Vogel, "A Text Book of Quantitative Inorganic Analysis", Longman, London, 1962.

[17] A. Angermann, J. Töpfer, Synthesis of magnetite nanoparticles by thermal decomposition of ferrous oxalate dihydrate, J. Mater. Sci., 43(15) (2008) 5123-5130.

[18] M. E. D. Thies-Weesie, A. P. Philipse , S. J. M. Kluijtmans, Preparation of sterically stabilized silica-hematite ellipsoids: sedimentation, permeation, and packing properties of prollate colloids, J. Colloids Interf. Sci., 174 (1995) 211-223.

[19] H. P. Klug, L.E. Alexander, "X-ray diffraction procedures", Wiley, New York (1970).

[20] [20] Y Haradayx, T Asakur, Dynamics and dynamic light-scattering properties of Brownian particles under laser radiation pressure , Pure Appl. Opt.7 (1998) 1001–1012

[21] R. D. Waldron, Infrared Spectra of Ferrites, Phys. Rev., 99 (1955) 1727-1735.

[22] R. Cornelland, U. Schwertmann, " The Iron Oxides", Wiley VCH Gmbh & Co. J GaA, 2nd edition, (2003).

[23] J. W. Park, E.H. Chae, S.H. Kim, J.H. Lee, J.W. Kim, S.M. Yoon, J. Y. Choi, Preparation of fine Ni powders from nickel hydrazine complex, Mater. Chem. Phys., 97 (2006) 371-378.

[24] E. A. Abdel-Aal, S. M. Malekzadeh, M. M. Rashad, A. A. El-Midany, H. El-Shall, Effect of synthesis conditions on preparation of nickel metal nanopowders via hydrothermal reduction technique, Powd. Technol., 171 (2007) 63-68.

[25] S. H. Gee, Y. K. Hong, D. W. Erickson and M. H. Park, Synthesis and aging effect of spherical magnetite (Fe_3O_4) nanoparticles for biosensor applications, J. Appl. Phys., 93 (2003) 7560-7562.

[26] M. Mousa, Gamma-irradiation effects on the electrical conductivity of pure and Cu- doped Fe3O4 spinel, J. Radioanal. Nucl. Chem., 118 (1987) 33-43.

[27] D. Thapa, V.R Palkar, M.B Kurup, S.K Malik, Properties of magnetite nanoparticles synthesized through a novel chemical route, Mater. Lett., 58 (2004) 2692-2694.

[28] R. B. Gupta, U. B. Kompella, "Nanoparticle Technology for Drug Delivery",Taylor &Francis, New York, (2006).